

**A Spitzer IRAC Imaging Survey for T Dwarf Companions  
Around M, L, and T Dwarfs:  
Observations, Results, and Monte Carlo Population Analyses**

J. C. Carson

College of Charleston, Department of Physics & Astronomy, 58 Coming St., Charleston,  
SC 29424, USA

M. Marengo

Iowa State University, Department of Physics and Astronomy, A313E Zaffarano, Ames, IA  
50011 USA

B. M. Patten

Harvard-Smithsonian Center for Astrophysics, 60 Garden St., Cambridge, MA 02138, USA

K. L. Luhman<sup>1</sup>

Pennsylvania State University, Department of Astronomy & Astrophysics, 525 Davey Lab,  
University Park, PA 16802, USA

S. M. Sonnett

University of Hawaii, Institute for Astronomy, 2680 Woodlawn Dr., Honolulu, Hawaii  
96822, USA

J. L. Hora, M. T. Schuster<sup>2</sup>

Harvard-Smithsonian Center for Astrophysics, 60 Garden St., Cambridge, MA 02138, USA

P. R. Allen

Franklin and Marshall College, Department of Physics and Astronomy, Lancaster, PA  
17604, USA

G. G. Fazio

Harvard-Smithsonian Center for Astrophysics, 60 Garden St., Cambridge, MA 02138, USA

J. R. Stauffer

Spitzer Science Center, 1200 E California Blvd., Pasadena, CA 91106, USA

C. Schnupp

Max-Planck-Institut für Astronomie, Königstuhl 17, 69117 Heidelberg, Germany

Received \_\_\_\_\_; accepted \_\_\_\_\_

Accepted for publication in the *Astrophysical Journal*.

---

<sup>1</sup>Center for Exoplanets and Habitable Worlds, The Pennsylvania State University, University Park, PA 16802

<sup>2</sup>Current Affiliation: Lincoln Laboratory, Massachusetts Institute of Technology, 244 Wood Street, Lexington, MA 02420

## ABSTRACT

We report observational techniques, results, and Monte Carlo population analyses from a *Spitzer* Infrared Array Camera imaging survey for substellar companions to 117 nearby M, L, and T dwarf systems (median distance of 10 pc, mass range of 0.6 to  $\sim 0.05 M_{\odot}$ ). The two-epoch survey achieves typical detection sensitivities to substellar companions of  $[4.5 \mu\text{m}] \leq 17.2$  mag for angular separations between about  $7''$  and  $165''$ . Based on common proper motion analysis, we find no evidence for new substellar companions. Using Monte Carlo orbital simulations (assuming random inclination, random eccentricity, and random longitude of pericenter), we conclude that the observational sensitivities translate to an ability to detect 600-1100K brown dwarf companions at semimajor axes  $\gtrsim 35$  AU, and to detect 500-600K companions at semimajor axes  $\gtrsim 60$  AU. The simulations also estimate a 600-1100K T dwarf companion fraction of  $< 3.4\%$  for 35-1200 AU separations, and  $< 12.4\%$  for the 500-600K companions, for 60-1000 AU separations.

*Subject headings:* methods: numerical — methods: statistical — stars: low-mass, brown dwarfs — stars: late-type — stars: binaries — infrared: stars

## 1. Introduction

A variety of mechanisms have been proposed for brown dwarf formation. For example, brown dwarfs might form in a similar manner as stars, by the direct collapse and fragmentation of molecular clouds. While standard cloud fragmentation theory has difficulty explaining the formation of such objects (Boss 2001; Bate et al. 2003), modified versions, such as those including supersonic magneto-turbulence, have the potential to produce the local high densities required for brown dwarf formation (Padoan & Nordlund 2004). An alternative theory is that photoevaporation by the ionizing radiation from nearby massive stars prematurely halts the accretion of what would otherwise be a more massive star, such as an F, G, K, or M type (Kroupa & Bouvier 2003; Whitworth & Zinnecker 2004). Finally, brown dwarfs could form through instabilities in the outer ( $\gtrsim 100$  AU) disk around a star, and then be pushed into the field by secular perturbations (Goodwin & Whitworth 2007; Stamatellos et al. 2007). In this scenario, brown dwarf formation more closely resembles planet formation than traditional star formation. In summary, the numerous models span a diversity of mechanisms, ranging from those most similar to star formation to those analogous to planet formation.

Multiplicity may be a powerful tool to test some formation mechanisms, because several theories argue that dynamical interactions may be essential for the formation of brown dwarfs (Reipurth & Clarke 2001; Boss 2001; Bate et al. 2002; Delgado-Donate et al. 2003; Umbreit et al. 2005; Goodwin & Whitworth 2007; Stamatellos et al. 2007). In Reipurth & Clarke (2001) for instance, the dynamical evolution of a group of protostars causes a member to be ejected from the natal cloud core, before the member can otherwise reach the Jeans mass necessary to form a star. Such scenarios would make it difficult to produce wide-separation, ( $>20$  AU) low-mass binaries. However, several examples of wide binary brown dwarfs have been discovered in recent years (Luhman 2004; Luhman et al.

2009, references therein). These observational discoveries, and others like them, therefore have the ability to constrain or perhaps disprove many ejection scenarios.

While individual discoveries are intriguing, providing accurate multiplicity statistics, in a consistent fashion, is necessary to rigorously test predictions of formation theories. A number of large-scale imaging surveys, ranging from optical wavelengths through the mid-infrared, have been carried out to help advance this effort (e.g. see Burgasser et al. 2007, Gelino et al. 2011, and references therein). However, for the coldest temperature brown dwarfs ( $<800\text{K}$ ), the  $4.5\ \mu\text{m}$  wavelength band of the Infrared Array Camera (IRAC; Fazio et al. 2004) on the *Spitzer Space Telescope* (Werner et al. 2004) offers the best sensitivities of any currently available instrument, as long as the companion is well distinguished from the primary star’s point spread function (PSF) (Patten et al. 2006). Large-scale IRAC multiplicity surveys, such as the multi-epoch study described in this paper, provide a powerful tool for probing the multiplicity of the coldest temperature objects. In this regard, surveys like ours can probe a phase space (cold temperatures, wide separations) inaccessible by alternative surveys focused on near-infrared and optical imaging, Doppler spectroscopy, or transit photometry. Accompanying Monte Carlo population analyses allow for rigorous population statistics to be drawn from the observational results.

Sections 2, 3, and 4 of this paper describe the target sample, observations, and data analysis, respectively, for this *Spitzer* IRAC observational survey. Section 5 summarizes the observational sensitivities. Section 6 discusses the Monte Carlo simulations. Section 7 summarizes the investigation.

## 2. Target List

For our target list, we selected 117 nearby ( $< 50$  pc) bright M, L, and T dwarfs for imaging with IRAC. The sample was designed to be a reasonably large collection of easily observable low mass (M, L, and T) stars and brown dwarfs that would allow one to constrain the frequency of wide, low-mass binaries. Out of the 117 targets, 31 are known multiple systems (see Table 1 for individual references). This value includes resolved and unresolved multiple systems as well as single stars with known narrow-separation planets, as determined from Doppler spectroscopy surveys. The observations were carried out between 2003 and 2009. Table 1 summarizes the target spectral types, *Spitzer* program identification (PID) numbers, distances (from parallax and spectral type fitting), and multiplicity information. The primary stars consist of 52 M dwarfs, 37 L dwarfs, and 28 T dwarfs. The distances range from 1.3 pc to 43.8 pc with a median distance of 9.9 pc. A rigorous calculation of the mass range of these primaries requires information on both target spectral type as well as age, and our system ages are largely unknown. However, a Bayesian analysis of local solar neighborhood late-M, L, and T dwarfs by Allen et al. (2005) reports mean masses as a function of brown dwarf spectral subtype, based on Burrows et al. (2001) evolutionary models. If we apply those statistical trends to our target list, along with Baraffe & Chabrier (1996) mass/spectral-type relations for the early M dwarfs, we estimate that our primaries have a mass range of 0.6 to  $\sim 0.05 M_{\odot}$ . As shown in Table 1, about 30% of the targets have no published distance measurements. For these targets, we approximated a distance based on the 4.5  $\mu\text{m}$  magnitude, spectral type, and magnitude-spectral-type trends reported in Patten et al. (2006). The magnitude-spectral-type technique results in typical distance errors of around 10%, when tested on target stars with known parallaxes. The fitted distance might be unreliable for individual targets, because unresolved binarity can affect the magnitude for a given spectral type. However, over a large ( $>100$ ) target population, they are adequate for delivering accurate statistics on the distance distribution.

Hence, distance uncertainties should have no significant adverse effects on our Monte Carlo companion statistics.

The target selection criteria used to plan the original PID 33 and 35 observing programs have the following biases: 1) a focus on relatively bright sources that accommodate high signal-to-noise (S/N) photometry of the primary; 2) an emphasis on relatively uncrowded fields; 3) a priority toward targets with known trigonometric parallaxes; and 4) an effort to avoid small-separation ( $\leq 6''$ ) binaries. Section 6 discusses how these biases might affect our multiplicity statistics.

The first epoch observations of the 117 targets were performed in *Spitzer* programs 33 and 35. Second epoch follow-up observations were carried out in PID 50013, 30298, 60046, 3736, 70021, and 30179 programs. The motivation for focusing on multi-epoch targets was the capability of using common proper motion as a measurement for bound companionship. Only one of the targets from the PID 33 and PID 35 programs, 2MASS J17281150+3948593, lacked a second epoch observation. Three targets from our original list, DENIS J153941.8-052042, 2MASS J07171626+5705430, and 2MASS J03480365+2344114, had second epoch observations, but with insufficient proper motion to enable an astrometric test for bound companions. We decided to discard 2MASS J03480365+2344114, due to significant controversies in its distance and multiplicity (Kirkpatrick et al. 1999), as well as the inadequate second epoch measurements. We retained the three remaining non-ideal targets in order to keep the original target sample as intact as possible. To identify T dwarf companions using only one epoch of IRAC data, we used photometry in four IRAC bands to perform a color-color identification (see Luhman et al. 2007, Marengo & Sanchez 2009). Such an analysis is usually limited by the IRAC 5.8  $\mu\text{m}$  sensitivities, due to a combination of high thermal background as well as a declining T-dwarf brightness at this wavelength (Patten et al. 2006). Common proper motion analysis only requires detections in one

photometric band, so we have the advantage of focusing on the  $4.5 \mu\text{m}$  region, which is the most sensitive IRAC band for T-dwarf detection. This equates to an effective sensitivity floor  $> 2$  magnitudes deeper (at  $4.5 \mu\text{m}$ ), as determined for targets with and without common proper motion data. The superior  $4.5\mu\text{m}$  sensitivities derives from a combination of low thermal background and a maximum brightness for late T dwarfs (see Patten et al. 2006).

### 3. Observations

The 117 targets were observed between 2003 and 2009 with the IRAC camera on the *Spitzer Space Telescope*. The IRAC plate scale and field of view are  $1.''2/\text{pixel}$  and  $5.'2 \times 5.'2$ , respectively (Fazio et al. 2004). The IRAC full width at half maximum (FWHM) at  $4.5 \mu\text{m}$  is  $1.''6$ . With the exception of 2MASS J17281150+3948593, all targets were observed in at least two epochs. Of the the two-epoch targets, all but DENIS J153941.8-052042 and 2MASS J07171626+5705430 exhibited  $\geq 0.''5$  of proper motion between observations. A motion of  $0.''5$ , equivalent to about one-third of a FWHM, was the minimum shift in a point source’s PSF where we found we could confidently check for co-movement with the primary, the test for a physically bound companionship. The first epoch observations were collected in all four IRAC channels ( $3.6$ ,  $4.5$ ,  $5.8$ , and  $8.0 \mu\text{m}$ ) while the second epoch observations were taken only at  $4.5$  and  $8.0 \mu\text{m}$ . For the common proper motion analysis, we focused only on the  $4.5 \mu\text{m}$  data, because of its superior sensitivity for late T dwarf detections. The observations at  $4.5 \mu\text{m}$  for PID 33, 35, 50013, 30298, 70021, and 60046 were performed in the manner described by Patten et al. (2006). For the cases of 2MASS J17281150+3948593, 2MASS J07171626+5705430, and DENIS J153941.8-052042 (all from PID 35), where proper motion tests were not possible, we used data collected in all four IRAC bandwidths, as described in Patten et al. (2006), to perform a color-color identification of possible



substellar companions. Data from PID 30179 was used for 2MASS J15344984-2952274, 2MASS J07271824+1710012, GJ 570 D, and 2MASS J04151954-0935066. These target observations from PID 30179 all used 26.8 second exposure times, net integration times of 214.4 seconds, and a 5-position dither pattern distributed within a  $13.''2$  radius. PID 3736 data, which included SDSS J125453.90-012247.4 and 2MASS J15074769-1627386, used a 10-point and 16-point dither pattern, respectively, distributed within a  $143''$  dither radius. Individual frame times were 26.8 and 10.4 seconds, respectively, with net integration times of 536 and 197.6 seconds. About a dozen targets exhibited saturation in the  $4.5 \mu\text{m}$  images. The saturation radius reached a maximum of  $4''$ .

## 4. Data Analysis

### 4.1. Image Reduction

Basic data reduction for all the observations was performed with the Spitzer Science Center (SSC) IRAC Pipeline (version S14.0.0), which produced Basic Calibrated Data (BCD) frames and data quality masks for each individual exposure. We used the post-BCD IRACproc package (Schuster et al. 2006) to obtain, for each target, a single flux calibrated mosaic combining all the individual exposures in each epoch for a given filter. Using a bilinear interpolation, IRACproc mapped the final mosaics onto a pixel grid with  $0.''86/\text{pixel}$  resolution. The effective field of view for object identification was  $5.''2 \times 5.''2$ . IRACproc makes use of the SSC mosaic software MOPEX and provides enhanced outlier (cosmic ray) rejection. Figure 1 shows an example of a reduced  $4.5 \mu\text{m}$  image.

## 4.2. Companion Identification

For each target, we used the task *starfind* within IRAF to measure astrometry for all point sources in the 4.5  $\mu\text{m}$  images from the first- and second-epoch observations. We matched the resulting source lists between the two epochs and used the average differences in right ascension and declination to correct for any offsets in the coordinate systems of the two epochs (which were usually less than  $\sim 0.2''$ ). To identify possible companions to a given target, we checked for sources with motions that were consistent with the motion expected for the primary based on its known proper motion and the time baseline between the two epochs. We also verified that the published proper motion of the primary agreed with the value that we measured using the IRAC data. For the 114 targets where a common proper motion analysis was possible, we did not identify any new companions to the primaries.

For 2MASS J17281150+3948593, 2MASS J07171626+5705430, and DENIS J153941.8-052042, where suitable second epoch data were not available, we searched for substellar companions based on a comparison of candidate magnitudes and colors using all four IRAC bands. The photometric analysis was carried out in a manner described by Patten et al. (2006). This included a photometry aperture radius of 4 native IRAC pixels and a sky annulus extending from 10 to 20 native IRAC pixels. These parameters were applied for all IRAC bands. We tested for a substellar identification using a photometric  $k$ -NN analysis described in Marengo & Sanchez (2009). The  $k$ -NN technique operates by defining an appropriate metric in the color and magnitude multidimensional space, and determines a “score” for each object, based on its “distance” from the colors and magnitudes of known T dwarfs. This method has been successful in identifying brown dwarf candidates in other *Spitzer* IRAC data, which were then confirmed with proper motion analysis (Luhman et al. 2007). However, it is unreliable at identifying substellar candidates when spectral type

is earlier than T3.

We required a  $\geq 5\sigma$  detection in all four IRAC channels in order for a source to be considered a viable candidate. No four-channel candidates exhibited colors and magnitudes consistent with a brown dwarf spectral type of T3 or later. The four-channel  $k$ -NN analysis was originally performed on all targets, before the second-epoch observations were carried out, and the more powerful common proper motion analysis became possible.

## 5. Observational Sensitivities

Our sensitivity to companions at narrow separations is limited most strongly by the primary star flux. At wider separations, the sensitivities are limited by a combination of incident field stars, zodiacal flux levels, and photon noise. For separations from the primary of  $30''$  and greater, we estimated sensitivities based on the standard deviations of flux levels from the frames in the dither pattern. Since we are most interested in a statistical representation of sensitivity levels, we did not measure wide-separation sensitivities for all 117 images, but rather determined flux level deviations for a representative sample (covering a range of zodiacal levels) and then extrapolated to the complete set.

Because we have difficulty detecting companions at the positions of field stars, we assumed that no brown dwarf identification could be made within two FWHM of a field star. We used this approach to determine a reasonably accurate incompleteness fraction that could be incorporated into the subsequent Monte Carlo simulations. At narrow separations ( $<30''$ ) from the primary, we used only the final combined image, and estimated sensitivities based on the standard deviation of flux inside concentric annuli centered on the primary star. The thickness of each annulus was one FWHM. It is likely that this method of determining high-contrast sensitivity over-estimates the noise somewhat, since

asymmetries in the primary star PSF may be interpreted as noise. For the purposes of our statistical analysis however, these sensitivity limits served as a quantifiable and useful tool to give us a conservative measurement of our ability to identify low mass companions at narrow separations.

Figure 2 shows our sensitivity curves, as compiled from the survey’s median, best 15%, and worst 15% of observations. Best and worst levels are based on measured sensitivities between 8 and 15 arcseconds from the primary and are affected by primary star brightness, field star density, and zodiacal background levels. In the cases of two-epoch data when one epoch had better sensitivities than the other, we adopted the sensitivity levels of the worse epoch. For the median curve, the  $5\sigma$  limiting magnitudes imply a sensitivity to substellar companions  $\sim 600\text{K}$  or warmer, for separations  $> 7''$  (assuming brown dwarf temperature-magnitude relations from Golimowski et al. 2004 and Patten et al. 2006).

## 6. Monte Carlo Population Simulations

To derive companion statistics from the observational data, we used Monte Carlo simulations combined with Bayesian modeling as described in Carson et al. (2006). For 2MASS J07171626+5705430, DENIS J153941.8-052042, and 2MASS J17281150+3948593, where brown dwarf companion identifications were carried out using a color-color analysis, instead of common proper motions, we used the  $5.8 \mu\text{m}$  final images, which were the least sensitive of the four and therefore dictated the achievable sensitivities for that analysis. For all other targets, we generated sensitivity maps from the  $4.5 \mu\text{m}$  reduced images using the protocol described in the previous section. The sensitivity maps served as inputs to the Monte Carlo simulations. Following Carson et al. (2006), we assumed, as a baseline configuration, that potential companions have a random eccentricity (between 0 and 0.9), random inclination, and random longitude of pericenter. The Monte Carlo simulations use

discrete steps to cover the range of possible companion orbital parameters. In our case, we sampled semimajor axes of 10, 20, 30, 40, 80, 100, 200, 400, 600, 800, 1000, 2000, 4000, 6000, and 10000 AU, and companion temperatures of 525, 633, 850, 950, and 1100 K. We chose these values because they provided a balance between a wide range of parameter space and an adequately small step size.

### 6.1. Detection Probabilities

Figure 3, generated from the Monte Carlo simulations, displays the likelihood of our detecting a substellar companion of a given temperature around a typical target (if a companion does indeed exist) as a function of semimajor axis. These curves take into account orbital projection effects (including the variations in time spent at different parts of the orbit) as well as survey sensitivities. For this plot, we assume a conversion between brown dwarf temperature and IRAC magnitude using relations in Patten et al. (2006) and Golimowski et al. (2004); Patten et al. (2006) allows for the conversion from IRAC magnitude to spectral subtype and Golimowski et al. (2004) allows for the conversion from spectral subtype to temperature. Figure 3 indicates that a 600-1100K companion with a semimajor axis somewhere between 35 and 1200 AU has a 60% chance of being detected in a given target observation, while a 500-600K companion between 60 and 1000 AU has a 16% chance of being detected. For the displayed plot, we selected the two temperature bins in order to present effective sensitivities for both relatively bright brown dwarfs, as well as fainter brown dwarfs that lie near the fringes of our sensitivity limits. The semimajor axis boundaries, quoted above, correspond to points on the curve where detection probabilities drop to around 50 to 60% of the peak probability levels.

Figure 4 shows the detection probabilities for a combined 500-1100K sample companion population (uniformly distributed across temperature). The plot also displays how detection

probabilities are affected if the hypothetical population is skewed toward circular orbits or highly eccentric orbits. A highly eccentric population translates into a sensitivity to smaller semimajor axes than for the case of more circular orbits. This is due to the fact that an orbiting companion with a high eccentricity spends a proportionately larger fraction of its orbit at separations exceeding the semimajor axis.

For the brown dwarf temperature and semimajor axis range that we are considering, there is no observational evidence, either in our data or in the published literature, that suggests a variation in the relative frequency of companions as a function of temperature. Because of this unknown, we assume a flat distribution of brown dwarf companion frequency versus temperature. However, Figure 5 displays detection probabilities for a combined 500-1100K sample, if we instead assume that the relative frequency of brown dwarf companions with temperature mimics that of the field brown dwarf distribution, as concluded by Bayesian analyses in Allen et al. (2005). In this modified case, the peak detection probability decreases by about 10%, owing to the input of a brown dwarf distribution where colder companions are more frequent than warmer ones.

## 6.2. Population Upper Limits

Following the Bayesian analysis described in Carson et al. (2006), a companion fraction upper limit was derived from the detection probability curves. Figure 6 shows 90% certainty upper limits to the fraction of systems with 600-1100K and 500-600K companions. The plot indicates that, at a 90% confidence level, at most 3.4% of survey targets have an undetected 600-1100K companion between 35 and 1200 AU. At most 12.4% of survey targets have an undetected 500-600K companion between 60 and 1000 AU (these upper limit values translate to 4.4% and 16.1%, respectively, for a 95% certainty calculation).

We decided to report the companion statistics for a constrained temperature range, as opposed to a mass range, because: 1) temperature is more directly observable than mass, and 2) the target sample contains biases which more strongly affect mass-constrained statistics than temperature-constrained statistics. Since brown dwarfs of a given mass grow fainter with age, Monte Carlo simulations that consider companion mass must incorporate theoretical evolutionary models as well as a-priori information on target system age. Most of the target stars in our sample have relatively unknown ages.

As described in Section 2, the target list contains known biases against small-separation ( $\leq 6''$ ) stellar binaries. In the case of temperature-constrained statistics, all such deselected systems have companion temperatures greater than the 500-1100K temperature range, and therefore do not affect derived statistics. But it is possible for a  $\leq 6''$  companion to affect mass-constrained statistics, since an unknown target system age implies a possible substellar mass overlapping with those explored by the Monte Carlo simulations. See Baraffe et al. (2003) for a discussion of the relationship between brown dwarf mass, age, and temperature.

The published substellar companions described in Table 1 come from a range of surveys and detection techniques (from Doppler spectroscopy to adaptive optics imaging) and hence contain a variety of detection biases. All of the published companions either have semimajor axes outside of those explored by the Monte Carlo simulations, or have temperatures outside of the 500-1100K range examined by our survey. Therefore, they do not affect temperature-constrained companion statistics. But due to the unknown ages of survey targets, some published companions, with semimajor axes probed by our Monte Carlo simulations, may have masses that are relevant to mass-constrained, companion statistics. Proper inclusion of such cases in a statistical analysis would therefore require a consideration of all published detections' observational biases. Such considerations are beyond the scope of this paper.

### 6.3. Comparison With Other Surveys

A wide variety of observational surveys have probed the question of multiplicity among low-mass stars and brown dwarfs (Burgasser et al. 2007). A recent statistical analysis on companions to low-mass stars and brown dwarfs is the investigation of Allen (2007). Taking into account observational biases and projection effects, that analysis combines the observational data from many different programs to conclude that the wide ( $\gtrsim 20$  AU) companion fraction to dwarfs of spectral-type M6 and later is no more than 1%-2%. This assumes a completeness to mass ratios as small as 0.5-0.7. As mentioned earlier, our analysis is defined by companion temperature, rather than mass. Hence, a direct comparison is difficult. However, around a typical target in our sample, the sensitivity floor of  $\sim 500\text{K}$  translates to an expected minimum mass ratio  $\sim 0.3$  (assuming Baraffe et al. 2003 evolutionary models and Allen et al. 2005 brown dwarf spectral-type/mass/age statistics). Hence, our companion fraction upper limit is generally consistent with the Allen (2007) result, and likely extends the wide-separation companion paucity to noticeably smaller companion masses and brightnesses.

## 7. Summary

Using IRAC on the *Spitzer Space Telescope*, we have conducted a substellar companion imaging survey of 117 nearby (median distance  $\sim 10$  pc) M, L, and T dwarf systems. Using  $4.5 \mu\text{m}$  imaging observations with multi-epoch common proper motion tests for the majority of targets, we achieved sensitivities to substellar companions as cool as  $\sim 500\text{K}$  for semimajor axes between 60 and 1000 AU; for  $>600\text{K}$  companions, we achieved sensitivities to semimajor axes ranging from 35 to 1200 AU. Our survey discovered no new companions. Based on the observational results, Monte Carlo population simulations determined that for the given target sample, the 600-1100K companion fraction is  $< 3.4\%$  for semimajor



axes of 35-1200 AU; the 500-600K companion fraction is  $< 12.4\%$  for semimajor axes of 60-1000 AU. We note that these Monte Carlo results represent the first rigorous statistics, among any parent star target class, of the wide separation ( $\geq 60$  AU)  $< 600$ K companion population.

The statistical results are consistent with previous studies that report a scarcity of wide-separation ( $> 30$  AU) substellar companions to low mass stars and brown dwarfs (e.g. Allen 2007, Burgasser et al. 2007). Our Monte Carlo results complement those previous studies by expanding companion statistics to include considerably lower temperature companions, for the given orbital separations. The Monte Carlo results are also consistent with brown dwarf formation models, such as ejection scenarios (see Section 1), that predict a scarcity of the widest and least massive binary systems. While our results are not comprehensive enough to definitely prove such theories, the unprecedented sensitivity and sample size will provide valuable constraints for the current and next generation of brown dwarf formation theories. Our study represents a constrained subset of a larger *Spitzer* IRAC companion search effort, which will be reported in a future publication.

We thank our referee, Angelle Tanner, for helpful comments which improved the manuscript. This work is based on observations made with the *Spitzer Space Telescope*, which is operated by the Jet Propulsion Laboratory (JPL), California Institute of Technology under a contract with NASA. Support for part of this work was provided by NASA through an award issued by JPL. Support for the IRAC instrument was provided by NASA under contract number 1256790 issued by JPL. J. C. C. was supported by grant AST-1009203 from the National Science Foundation. K. L. was supported by grant AST-0544588 from the National Science Foundation. The Center for Exoplanets and Habitable Worlds is supported by the Pennsylvania State University, the Eberly College of Science, and the Pennsylvania Space Grant Consortium. This research has made use of the

following databases: 1) the M, L, and T dwarf compendium housed at DwarfArchives.org and maintained by Chris Gelino, Davy Kirkpatrick, and Adam Burgasser; 2) the SIMBAD database, operated at CDS, Strasbourg, France; 3) the NASA/IPAC/NEExSci Star and Exoplanet Database, which is operated by JPL; and 4) the Washington Double Star Catalog maintained at the U.S. Naval Observatory.

*Facilities:* Spitzer (IRAC).

## REFERENCES

- Allen, P. R. 2007, *ApJ*, 668, 492
- Allen, P. R., Koerner, D. W., Reid, I. N., & Trilling, D. E. 2005, *ApJ*, 625, 385
- Baraffe, I., & Chabrier, G. 1996, *ApJ*, 461, L51
- Baraffe, I., Chabrier, G., Barman, T. S., Allard, F., & Hauschildt, P. H. 2003, *A&A*, 402, 701
- Bate, M. R., Bonnell, I. A., & Bromm, V. 2002, *MNRAS*, 332, L65
- Bate, M. R., Bonnell, I. A., & Bromm, V. 2003, *MNRAS*, 339, 577
- Boss, A. P. 2001, *ApJ*, 551, L167
- Bouy, H., Brandner, W., Martín, E. L., Delfosse, X., Allard, F., & Basri, G. 2003, *AJ*, 126, 1526
- Burgasser, A. J., Kirkpatrick, J. D., Cruz, K. L., Reid, I. N., Leggett, S. K., Liebert, J., Burrows, A., & Brown, M. E. 2006, *ApJS*, 166, 585
- Burgasser, A. J., Kirkpatrick, J. D., & Lowrance, P. J. 2005, *AJ*, 129, 2849
- Burgasser, A. J., Kirkpatrick, J. D., Reid, I. N., Brown, M. E., Miskey, C. L., & Gizis, J. E. 2003, *ApJ*, 586, 512
- Burgasser, A. J., Liu, M. C., Ireland, M. J., Cruz, K. L., & Dupuy, T. J. 2008, *ApJ*, 681, 579
- Burgasser, A. J., Reid, I. N., Siegler, N., Close, L., Allen, P., Lowrance, P., & Gizis, J. 2007, *Protostars and Planets V*, 427

- Burrows, A., Hubbard, W. B., Lunine, J. I., & Liebert, J. 2001, *Reviews of Modern Physics*, 73, 719
- Carson, J. C., Eikenberry, S. S., Smith, J. J., & Cordes, J. M. 2006, *AJ*, 132, 1146
- Delgado-Donate, E. J., Clarke, C. J., & Bate, M. R. 2003, *MNRAS*, 342, 926
- Delfosse, X., Forveille, T., Udry, S., Beuzit, J.-L., Mayor, M., & Perrier, C. 1999, *A&A*, 350, L39 2004, in *ASP Conf. Ser. 318, Spectroscopically and Spatially Resolving the Components of the Close Binary Stars*, ed. R. W. Hilditch, H. Hensberge, & K. Pavlovski (San Francisco: ASP), 166
- Fazio, G. G., et al. 2004, *ApJS*, 154, 10
- Gelino, C. R., Kulkarni, S. R., & Stephens, D. C. 2006, *PASP*, 118, 611
- Gelino, C. R., et al. 2011, *AJ*, 142, 57
- Gizis, J. E., Reid, I. N., Knapp, G. R., Liebert, J., Kirkpatrick, J. D., Koerner, D. W., & Burgasser, A. J. 2003, *AJ*, 125, 3302
- Golimowski, D. A., et al. 2004, *AJ*, 127, 3516
- Goodwin, S. P., & Whitworth, A. 2007, *A&A*, 466, 943
- Kirkpatrick, J. D., et al. 1999, *ApJ*, 519, 802
- Kroupa, P., & Bouvier, J. 2003, *MNRAS*, 346, 369
- Luhman, K. L. 2004, *ApJ*, 614, 398
- Luhman, K. L., et al. 2007, *ApJ*, 654, 570
- Luhman, K. L., Mamajek, E. E., Allen, P. R., Muench, A. A., & Finkbeiner, D. P. 2009, *ApJ*, 691, 1265

- Marengo, M., & Sanchez, M. C. 2009, *AJ*, 138, 63
- Mason, B. D., Wycoff, G. L., Hartkopf, W. I., Douglass, G. G., & Worley, C. E. 2001, *AJ*, 122, 3466
- McCaughrean, M. J., Close, L. M., Scholz, R.-D., Lenzen, R., Biller, B., Brandner, W., Hartung, M., & Lodieu, N. 2004, *A&A*, 413, 1029
- Montes, D., López-Santiago, J., Gálvez, M. C., Fernández-Figueroa, M. J., De Castro, E., & Cornide, M. 2001, *MNRAS*, 328, 45
- Nakajima, T., Oppenheimer, B. R., Kulkarni, S. R., Golimowski, D. A., Matthews, K., & Durrance, S. T. 1995, *Nature*, 378, 463
- Neuhäuser, R., et al. 2002, *Astronomische Nachrichten*, 323, 447
- Padoan, P., & Nordlund, Å. 2004, *ApJ*, 617, 559
- Patten, B. M., Stauffer, J. R., Burrows, A., Marengo, M., Hora, J. L., Luhman, K. L., Sonnett, S. M., Henry, T. J., Raghavan, D., Megeath, S. T., Liebert, J., & Fazio, G. G. 2006, *ApJ*, 651, 502
- Perryman, M. A. C., et al. 1997, *A&A*, 323, L49
- Reid, I. N., Gizis, J. E., Kirkpatrick, J. D., & Koerner, D. W. 2001, *AJ*, 121, 489
- Reipurth, B., & Clarke, C. 2001, *AJ*, 122, 432
- Scholz, R.-D., McCaughrean, M. J., Lodieu, N., & Kuhlbrodt, B. 2003, *A&A*, 398, L29
- Schroeder, D. J., et al. 2000, *AJ*, 119, 906
- Schuster, M. T., Marengo, M., & Patten, B. M. 2006, *Proc. SPIE*, 6270, 65S

Stamatellos, D., Hubber, D. A., & Whitworth, A. P. 2007, MNRAS, 382, L30 & Kasper, M. 2008, arXiv:0811.0556

Umbreit, S., Burkert, A., Henning, T., Mikkola, S., & Spurzem, R. 2005, ApJ, 623, 940

Werner, M. W., et al. 2004, ApJS, 154, 1

Wertheimer, J. G., & Laughlin, G. 2006, AJ, 132, 1995

Whitworth, A. P., & Zinnecker, H. 2004, A&A, 427, 299

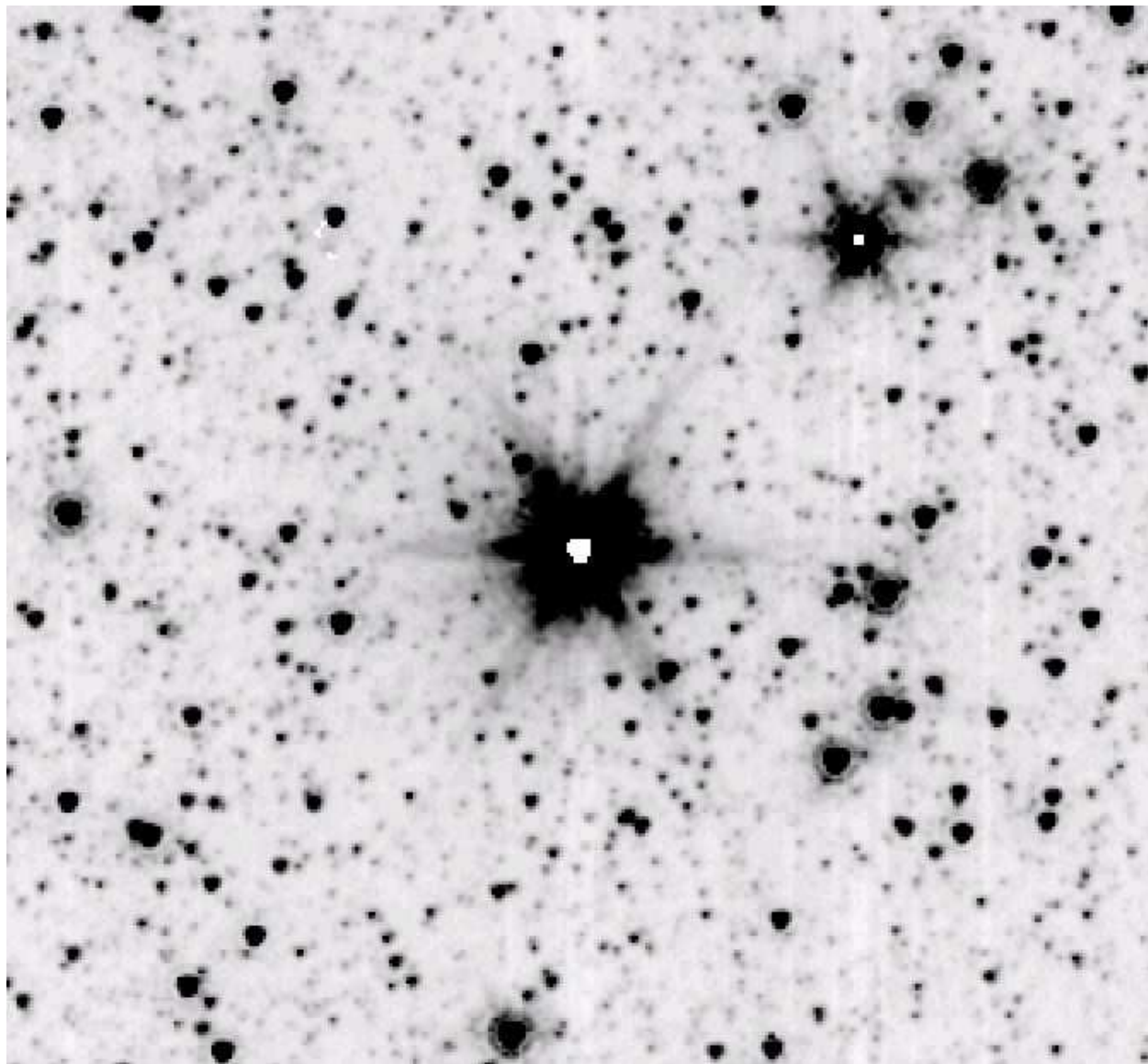


Fig. 1.— Reduced *Spitzer* IRAC 4.5  $\mu\text{m}$  image of GJ 551 (one of the brighter targets). Displayed field of view is  $\sim 4.8 \times 4.8$ . The white spot at the center of the bright star is due to saturation. The image illustrates how sensitivities to companions are affected by primary star brightness and incident field stars.

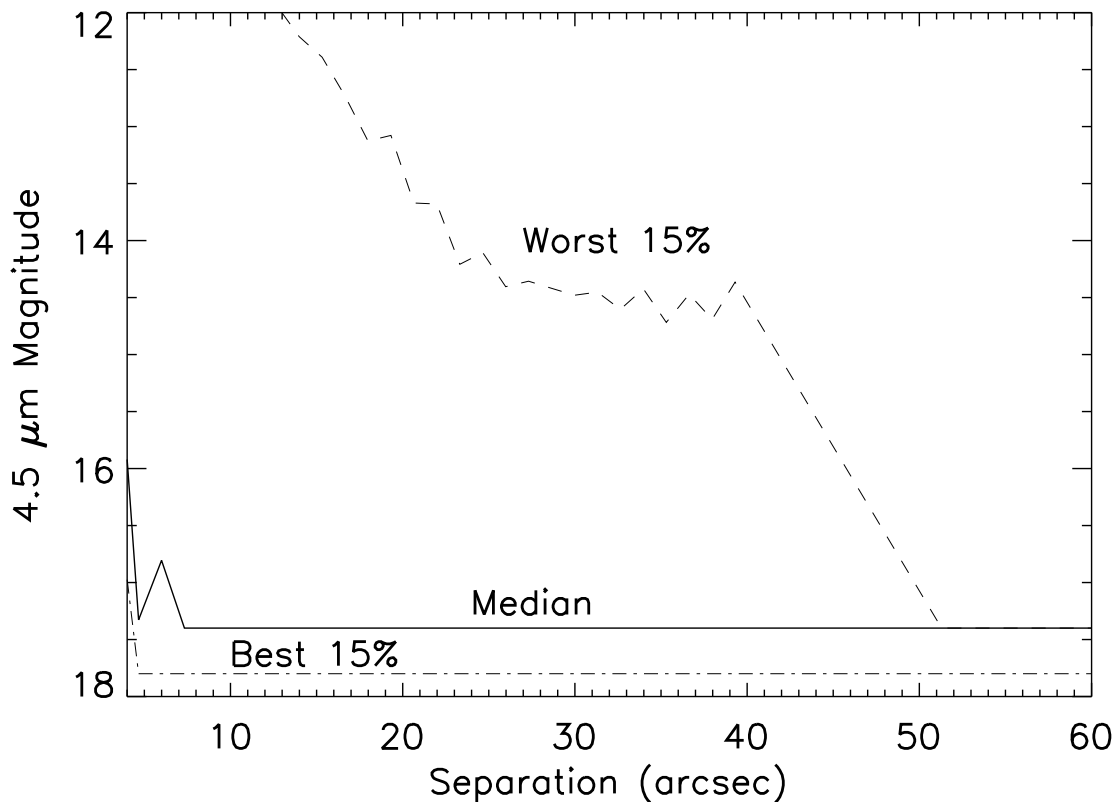


Fig. 2.— The  $4.5 \mu\text{m}$  sensitivity curves displaying limiting magnitude as a function of separation from the primary. The solid curve represents median survey sensitivities. The dashed curve represents median sensitivities for the worst 15% of observations. The dot-dashed curve represent median sensitivities for the best 15% of observations. All minimum magnitudes correspond to  $5\sigma$  detections. Outside of the halo of the primary, typically at  $\sim 7''$  separations, sensitivity estimates are purely a function of zodiacal background levels and field star density.



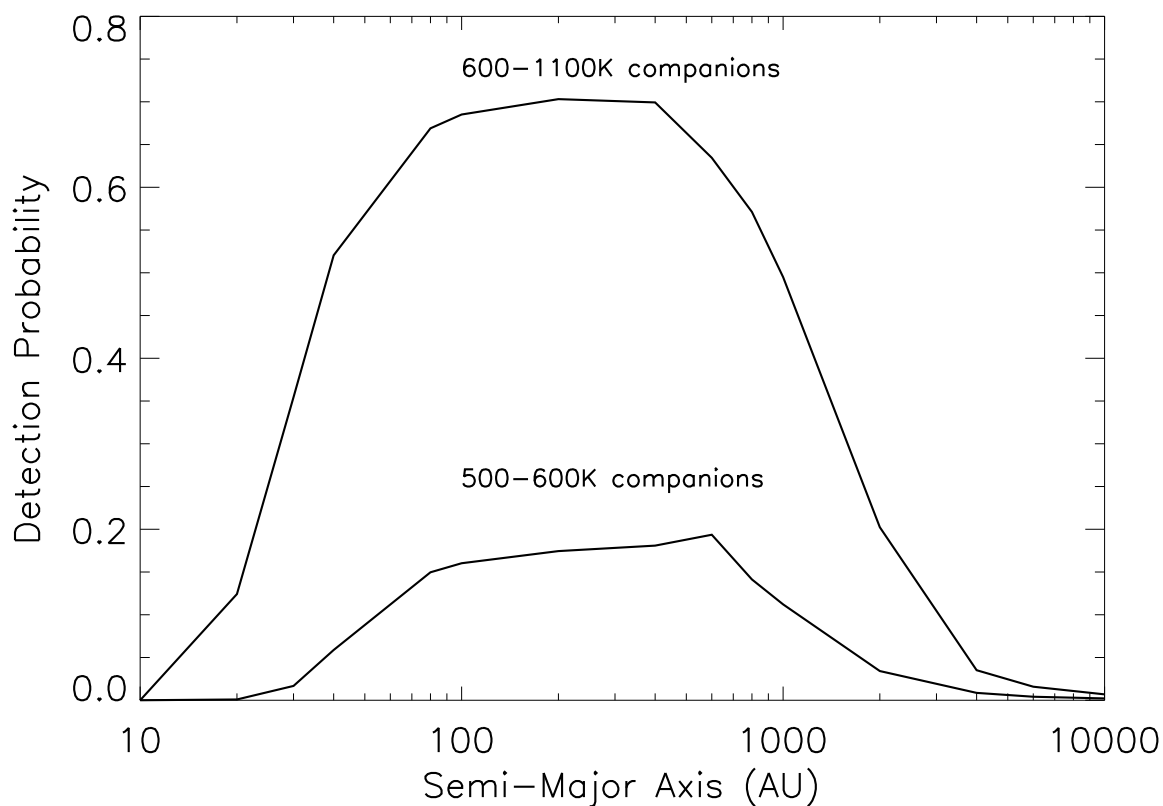


Fig. 3.— Detection probability versus semimajor axis for substellar companions, as output from Monte Carlo simulations. The plotted detection probability represents the likelihood that the survey successfully identifies a substellar companion, if one does indeed exist, as a function of companion semi-major axis. These curves represent an average over all survey observations. The top curve is the detection probability for 600-1100K companions and the bottom curve is the probability for 500-600K companions.

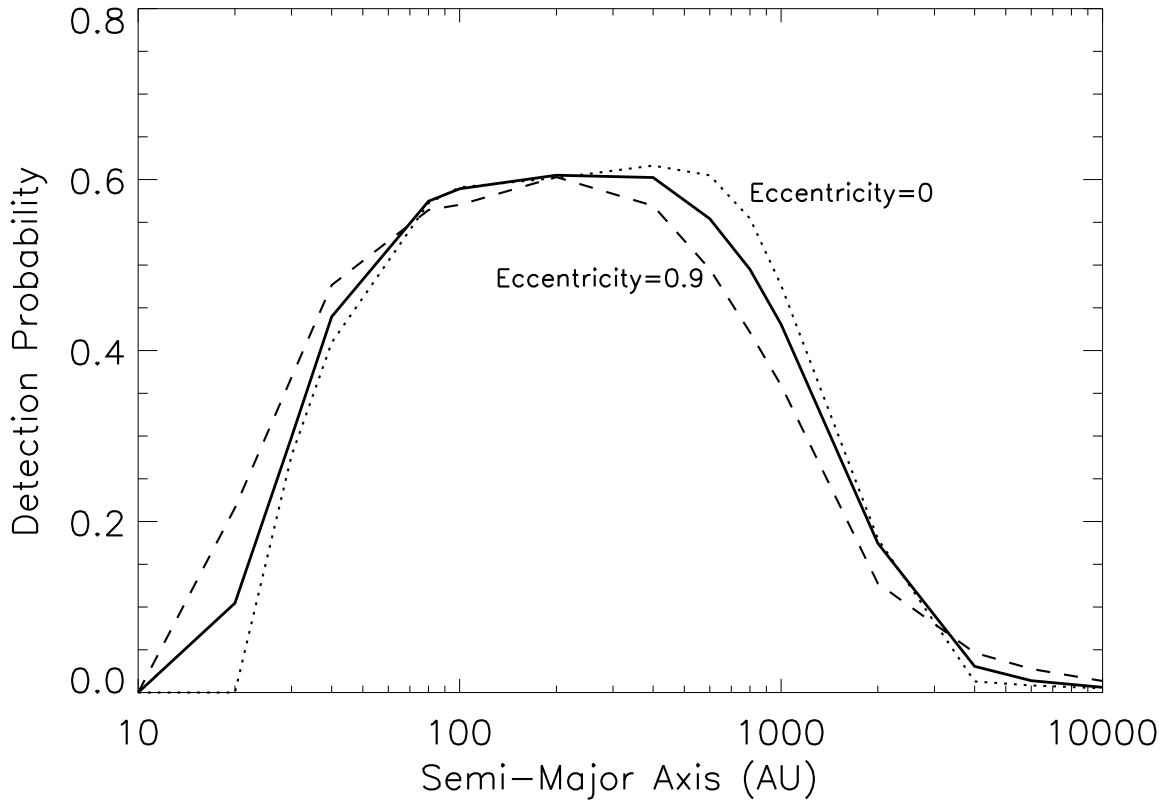


Fig. 4.— Detection probability versus semimajor axis for substellar companions, as output from Monte Carlo simulations. The solid curve indicates the detection probability for a uniform 500-1100K sample companion population with random eccentricity. (It is effectively a consolidation of the Figure 3 curves.) The dashed and dotted curves demonstrate how detection probabilities change when one assumes a highly eccentric ( $e=0.9$ ) or highly circular ( $e=0$ ) orbital population. Note that a highly eccentric companion population implies a sensitivity to narrower semimajor axes than a more circular companion population.

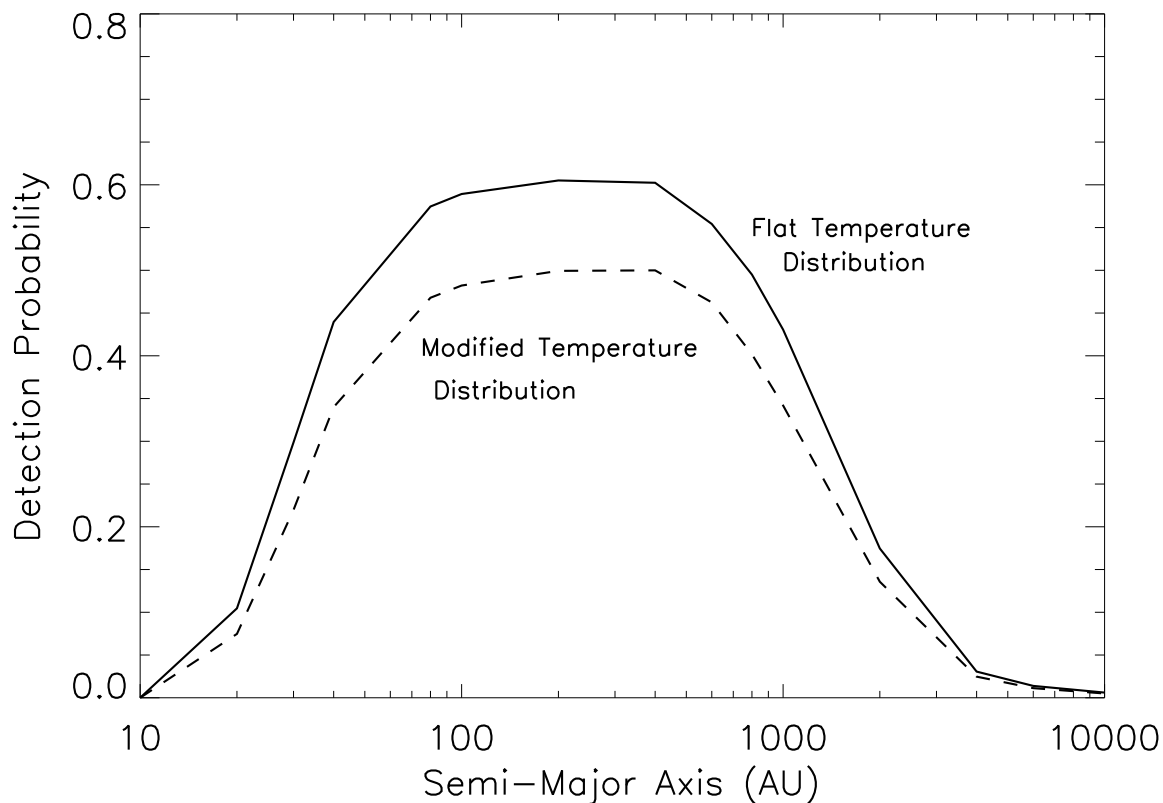


Fig. 5.— Detection probability versus semimajor axis for substellar companions, as output from Monte Carlo simulations. The solid curve indicates the detection probability for a uniform 500-1100K sample companion population where the relative frequency of brown dwarf companions varies flatly with temperature. (It is effectively a consolidation of the Figure 3 curves.) The dashed curve demonstrates how detection probabilities change when one assumes that the relative frequency of companion brown dwarfs versus temperature mimics closely that of field brown dwarf populations. Detection probabilities drop about 10% for the modified temperature distribution, owing to the higher relative frequency of colder, and therefore fainter, companions.

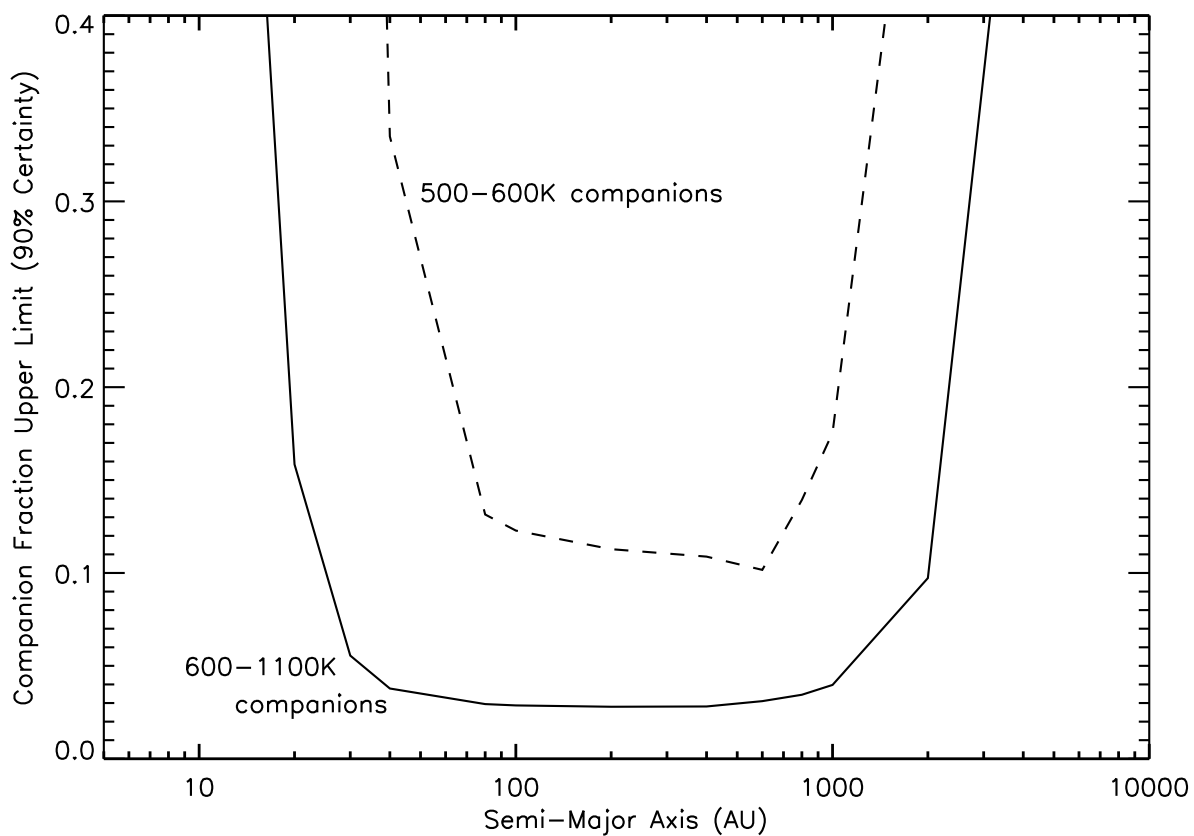


Fig. 6.— Upper limit for the frequency of brown dwarf companions, at a 90% confidence level, versus semimajor axis, as outputted by our Monte Carlo simulations. The upper curve shows statistical upper limits for 500-600K companions and the bottom curve shows upper limits for 600-1100K companions. The curves indicate that at most 3.4% of survey targets have an undetected 600-1100K companion between 35 and 1200 AU. At most 12.4% of survey targets have an undetected 500-600K companion between 60 and 1000 AU.

Table 1. Sample of Late-M, L, and T Dwarf Systems

Name	<i>Spitzer</i> PID Number	Spectral Type	Distance <sup>a</sup> (pc)	Multiplicity Notes <sup>b</sup>	Spectral Type Ref. [& Multiplicity Ref.]
GJ 825	33, 30298	M0	4.0		1
GJ 412 AB	33, 30298	M0.5+M5.5	4.8	binary; separation = 28'' (resolved)	2 [3,4]
GJ 229 AB	35, 30298	M1+T7	5.8	binary; separation = 7.''8	5 [5]
GJ 191	33, 30298	M1.5	3.9		1
GJ 15 AB	33, 30298	M1.5+M3.5	3.6	binary; separation = 34.''8 (resolved)	1 [1,4]
GJ 887	33, 30298	M1.5	3.3		1
GJ 411	33, 30298	M2	2.6		1
GJ 752 AB	35, 30298	M2+M8	5.9	binary; separation = 74'' (resolved)	2 [3,4]
GJ 1	33, 30298	M3	4.4		1
GJ 388	33, 30298	M3	4.7		1
GJ 628	33, 30298	M3	4.3		1
GJ 674	33, 30298	M3	4.5	known exoplanet from Doppler spectroscopy	1 [1]
GJ 687	33, 30298	M3	4.5		1
GJ 832	33, 30298	M3	4.9	known exoplanet from Doppler spectroscopy	1 [1]
GJ 860 AB	33, 30298	M3+M4	4.0	binary; separation = 3.''4	1 [1,6]
GJ 725 AB	33, 30298	M3+M3.5	3.6	binary; separation = 13.''3 (resolved)	1 [1]
GJ 729	33, 30298	M3.5	3.0		1
GJ 273	33, 30298	M3.5	3.8		1
GJ 876	33, 30298	M3.5	4.7	3 known exoplanets from Doppler spectroscopy	1 [1]
GJ 1001 A	35, 30298	M3.5	9.5 <sup>c</sup>	part of a triple system; 18.''2 (resolved) from BC	2 [7]
GJ 447	33, 30298	M4	3.3		1
GJ 699	33, 30298	M4	1.8		1

Table 1—Continued

Name	<i>Spitzer</i> PID Number	Spectral Type	Distance <sup>a</sup> (pc)	Multiplicity Notes <sup>b</sup>	Spectral Type Ref. [& Multiplicity Ref.]
GJ 54.1	33, 30298	M4.5	3.7		1
GJ 83.1	33, 30298	M4.5	4.5		1
GJ 234 AB	33, 30298	M4.5+??	4.1	binary; separation = 1.''3	1 [1,4]
GJ 866 ABC	33, 30298	M4.5+M5+M6 <sup>d</sup>	3.3	triple system; AC to B separation = 0.''35; A to C separation < 0.''1	8,9 [8]
GJ 1093	35, 30298	M5	7.8		2
GJ 1156	35, 30298	M5.5	6.5		2
GJ 1002	33, 30298	M5.5	4.7		2
LHS 288	33, 30298	M5.5	4.5		2
GJ 473 AB	33, 30298	M5.5+??	4.4	binary; separation = 0.''7	1 [1,4]
GJ 551	33, 30298	M5.5	1.3	part of a triple system; 16.''7 separation from a binary (outside field of view)	1 [10]
GJ 905	33, 30298	M5.5	3.2		1
GJ 1061	33, 30298	M5.5	3.7		1
GJ 1245 ABC	33, 30298	M5.5+M5.5+>M6	4.7	triple system; AB separation = 7.''0 (resolved); AC separation = 0.''6.	11 [11]
GJ 65 AB	33, 30298	M5.5+M6	2.7	binary; separation = 0.''7	1 [1,4]
GJ 406	33, 30298	M6	2.4		1
GJ 1111	33, 30298	M6.5	3.6		2
LHS 292	33, 30298	M6.5	4.6		2
SO 025300.5+165258	33, 50013	M7	3.7		2
LHS 3003	35, 30298	M7	6.4		2
GJ 644 C	35, 30298	M7	6.5	part of a triple system; C to A separation = 4.''9 (outside field of view)	2 [3,4]
LHS 132	35, 30298	M8	11.0 <sup>c</sup>		2
LHS 2021	35, 30298	M8	15.0 <sup>c</sup>		2

Table 1—Continued

Name	<i>Spitzer</i> PID Number	Spectral Type	Distance <sup>a</sup> (pc)	Multiplicity Notes <sup>b</sup>	Spectral Type Ref. [& Multiplicity Ref.]
2MASS J18353790+3259545	35, 30298	M8.5	5.7		2
2MASS J03202839-0446358	35, 30298	M8.5+T5	26.0 <sup>c</sup>	binary; separation < 0.''33	12 [12]
LP 944-020	33, 30298	M9	5.0		2
LHS 2065	35, 30298	M9	8.6		2
LHS 2924	35, 30298	M9	11.0		2
DENIS J104814.6-395606	33, 30298	M9	4.5 <sup>e</sup>		3
DENIS J002105.8-424442	35, 30298	M9.5	24.9 <sup>c</sup>		2
BRI 0021-0214	35, 30298	M9.5	11.5		2
2MASS J12043036+3212595	35, 70021	L0	43.8 <sup>c</sup>		2
2MASS J04510093-3402150	35, 60046	L0.5	28.0 <sup>c</sup>		2
2MASS J07464256+2000321 AB	35, 30298	L0.5+L	12.2	binary; separation = 0.''22	13 [13]
Kelu-1	35, 30298	L2+L3.5	18.5	binary; separation = 0.''37	14 [14]
2MASSW J1300426+191235	35, 30298	L1	14.6 <sup>c</sup>		2
2MASS J14392837+1929150	35, 30298	L1	14.3		2
2MASS J15551573-0956055	35, 30298	L1	13.8 <sup>c</sup>		2
2MASS J16452211-1319516	35, 30298	L1.5	13.3 <sup>c</sup>		2
2MASS J10170754+1308398	35, 60046	L2+earlyL	30.9 <sup>c</sup>	binary; separation = 0.''10	15 [15]
2MASS J11553952-3727350	35, 30298	L2	17.1 <sup>c</sup>		2
DENIS J105855.9-154814	35, 50013	L3	17.2		2
2MASS J1506544+132106	35, 30298	L3	11.4 <sup>c</sup>		2
2MASS J1721039+334415	35, 30298	L3	15.9 <sup>c</sup>		2
SDSS J202820.32+005226.5	35, 60046	L3	19.0 <sup>c</sup>		2

Table 1—Continued

Name	<i>Spitzer</i> PID Number	Spectral Type	Distance <sup>a</sup> (pc)	Multiplicity Notes <sup>b</sup>	Spectral Type Ref. [& Multiplicity Ref.]
2MASS J21041491-1037369	35, 30298	L3	15.7 <sup>c</sup>		2
2MASS J00361617+1821104	35, 30298	L3.5	8.8		2
DENIS J153941.8-052042	35, 30298	L4	16.0 <sup>c</sup>		2
2MASS J01410321+1804502	35, 30298	L4.5	16.7 <sup>c</sup>		2
2MASS J06523073+4710348	35, 60046	L4.5	8.8 <sup>c</sup>		2
2MASS J22244381-0158521	35, 30298	L4.5	11.4		2
SDSS J053951.99-005902.0	35, 30298	L5	13.2		2
2MASS J08354256-0819237	35, 30298	L5	6.7 <sup>c</sup>		2
2MASS J09083803+5032088	35, 30298	L5	14.0 <sup>c</sup>		2
2MASS J15074769-1627386	35, 3736	L5	7.4		2
GJ 1001 BC	35, 30298	L5+midL	9.5	binary; part of a triple system; B to C separation = 0.''09; BC to A separation = 18.''2 (resolved)	7 [7]
SDSS J133148.92-011651.4	35, 30298	L6	26.3 <sup>c</sup>		2
2MASSW J1515008+484742	35, 30298	L6	12.3 <sup>c</sup>		2
2MASS J07171626+5705430	35, 30298	L6.5	16.8 <sup>c</sup>		2
SDSS J042348.57-041403.5	35, 30298	L6.5+T2	15.2	binary; separation = 0.''16	16 [16]
2MASS J15261405+2043414	35, 30298	L7	25.2 <sup>c</sup>		2
2MASS J17281150+3948593	35	L7+L/T	24.4	binary; separation = 0.''13	17 [17]
2MASS J08251968+2115521	35, 30298	L7.5	10.6		2
DENIS J025503.3-470049	35, 30298	L8	7.2 <sup>c</sup>		2
SDSS J085758.45+570851.4	35, 30298	L8	13.3 <sup>c</sup>		2
GJ 337 CD	35, 30298	L8+~L8	20.4	part of a quadruple system; CD separation = 0.''53; AB to CD separation = 43'' (resolved)	18 [18]
2MASS J16322911+1904407	35, 30298	L8	15.2		2



Table 1—Continued

Name	<i>Spitzer</i> PID Number	Spectral Type	Distance <sup>a</sup> (pc)	Multiplicity Notes <sup>b</sup>	Spectral Type Ref. [& Multiplicity Ref.]
2MASS J05325346+8246465	35, 30298	sdL	8.4 <sup>c</sup>		2
SDSS J015141.69+124429.6	35, 30298	T0.5	21.3		2
SDSS J083717.22-000018.3	35, 50013	T1	29.4		2
$\epsilon$ Ind BC	33, 60046	T1+T6	3.6	binary; part of a triple system; BC separation = 0.''73; BC to A separation = 6.'7 (outside field of view)	2 [19,20]
SDSS J125453.90-012247.4	35, 3736	T2	11.8		2
SDSS J102109.69-030420.1	35, 50013	$\lesssim$ T2+T5	29.4	binary; separation = 0.''17	16 [16]
SDSS J175032.96+175903.9	35, 50013	T3.5	27.8		2
2MASS J22541892+3123498	35, 30298	T4	15.0 <sup>c</sup>		2
SDSS J020742.87+000056.0	35, 50013	T4.5	28.6		2
2MASS J05591914-1404488	35, 30298	T4.5	10.2		2
SDSS J092615.38+584720.9	35, 30298	T4.5 <sup>f</sup>	17.0 <sup>c</sup>	binary; separation = 0.''07	16 [16]
2MASS J07554795+2212169	35, 30298	T5	13.6 <sup>c</sup>		2
2MASS J23391025+1352284	35, 30298	T5	15.5 <sup>c</sup>		2
2MASSW J2356547-155310	35, 30298	T5	14.5		2
2MASS J15344984-2952274	35, 30179	T5.5 <sup>f</sup>	13.5	binary; separation = 0.''07	21 [21]
2MASS J15462718-3325111	35, 60046	T5.5	11.4		2
SDSS J111010.01+011613.1	35, 30298	T5.5	14.2 <sup>c</sup>		2
2MASS J02431371-2453298	35, 30298	T6	10.6		2
2MASS J12255432-2739466	35, 30298	T6+T8	13.3	binary; separation = 0.''28	21 [21]
SDSS J162414.37+002915.6	35, 30298	T6	11.0		2
2MASS J09373487+2931409	35, 30298	T6p	6.1		2
2MASSW J1047539+212423	35, 30298	T6.5	10.5		2

Table 1—Continued

Name	<i>Spitzer</i> PID Number	Spectral Type	Distance <sup>a</sup> (pc)	Multiplicity Notes <sup>b</sup>	Spectral Type Ref. [& Multiplicity Ref.]
2MASS J12373919+6526148	35, 30298	T6.5	10.4		2
SDSS J134646.45-003150.4	35, 30298	T6.5	14.7		2
2MASS J15530228+1532369	35, 30298	T6.5+T7	9.2 <sup>c</sup>	binary; separation = 0.''35	16 [16]
2MASS J07271824+1710012	35, 30179	T7	9.1		2
2MASS J12171110-0311131	35, 30298	T7.5	11.0		2
GJ 570 D	35, 30179	T7.5	5.9		2
2MASS J04151954-0935066	35, 30179	T8	5.8		2

Note. — Targets are sorted according to spectral type. The IRAC magnitudes of all the L and T-type targets, and most of the M-type targets, are published in Patten et al. (2006).

<sup>a</sup>Values from Patten et al. (2006), when available, or NASA/IPAC/NEExSci Star and Exoplanet Database (*NStED*; <http://nsted.ipac.caltech.edu>), unless otherwise noted.

<sup>b</sup>All multiple systems are unresolved unless otherwise noted.

<sup>c</sup>Distance approximated from 3.6  $\mu\text{m}$  magnitude, spectral type, and magnitude-spectral-type relations from Patten et al. (2006).

<sup>d</sup>Spectral types derived by authors using Delfosse et al. (1999) mass estimates and Baraffe & Chabrier (1996) mass/spectral-type relations.

<sup>e</sup>From Neuhäuser et al. (2002).

<sup>f</sup>Composite identification.

References. — (1) NASA/IPAC/NExScI Star and Exoplanet Database, <http://nsted.ipac.caltech.edu>; (2) Patten et al. 2006; (3) Montes et al. 2001; (4) Washington Double Star Catalog; Mason et al. 2001; (5) Nakajima et al. 1995; (6) Hipparcos; Perryman et al. 1997; (7) Golimowski et al. 2004; (8) Delfosse et al. 1999; (9) Baraffe & Chabrier 1996; (10) Wertheimer & Laughlin 2006; (11) Schroeder et al. 2000; (12) Burgasser et al. 2008; (13) Reid et al. 2001; (14) Gelino et al. 2006; (15) Bouy et al. 2003; (16) Burgasser et al. 2006; (17) Gizis et al. 2003; (18) Burgasser, Kirkpatrick, & Lowrance 2005; (19) McCaughrean et al. 2004; (20) Scholz et al. 2003; (21) Burgasser et al. 2003.